Molecular Neurobiology (2022) 59:161–176
https://doi.org/10.1007/s12035-021-02571-y

Ferrostatin-1 Alleviates White Matter Injury Via Decreasing Ferroptosis Following Spinal Cord Injury

Hongfei Ge[1] · Xingsen Xue[1] · Jishu Xian[1] · Linbo Yuan[1] · Long Wang[1] · Yongjie Zou[1,2] · Jun Zhong[1] · Zhouyang Jiang[1] · Jiantao Shi[1] · Tunan Chen[1] · Hong Su[1] · Hua Feng[1] · Shengli Hu[1]

Received: 8 April 2021 / Accepted: 15 September 2021 / Published online: 12 October 2021

Abstract

Spinal cord injury (SCI), a devastating neurological impairment, usually imposes a long-term psychological stress and high socioeconomic burden for the sufferers and their family. Recent researchers have paid arousing attention to white matter injury and the underlying mechanism following SCI. Ferroptosis has been revealed to be associated with diverse diseases including stroke, cancer, and kidney degeneration. Ferrostatin-1, a potent inhibitor of ferroptosis, has been illustrated to curb ferroptosis in neurons, subsequently improving functional recovery after traumatic brain injury (TBI) and SCI. However, the role of ferroptosis in white matter injury and the therapeutic effect of ferrostatin-1 on SCI are still unknown. Here, our results indicated that ferroptosis played a pivotal role in the secondary white matter injury, and ferrostatin-1 could reduce iron and reactive oxygen species (ROS) accumulation and downregulate the ferroptosis-related genes and its products of IREB2 and PTGS2 to further inhibit ferroptosis in oligodendrocyte, finally reducing white matter injury and promoting functional recovery following SCI in rats. Meanwhile, the results demonstrated that ferrostatin-1 held the potential of inhibiting the activation of reactive astrocyte and microglia. Mechanically, the present study deciphers the potential mechanism of white matter damage, which enlarges the therapeutic effects of ferrostatin-1 on SCI and even in other central nervous system (CNS) diseases existing ferroptosis.

Keywords Spinal cord injury · Ferroptosis · White matter injury · Reactive oxygen species · Ferrostatin-1

Abbreviations

SCI	Spinal cord injury
TBI	Traumatic brain injury
ROS	Reactive oxygen species
CNS	Central nervous system
ASIC 1a	Acid-sensing ion channel 1a
GPER1	G-protein coupled estrogen receptor 1
NSCs	Neural stem cells
DFX	Deferoxamine
DMT1	Divalent metal transporter 1
RCD	Regulated cell death
BBB	Blood–brain barrier
OPCs	Oligodendrocyte progenitor cells
DMEM	Dulbecco's modified Eagle's medium
PDGF	Platelet-derived growth factor
PBS	Phosphate-buffered saline
IHC	Immunohistochemistry
DAB	3-Diaminobenzidine
BCA	Bicinchoninic acid
HRP	Horseradish peroxidase
RT-qPCR	Reverse transcription-quantitative polymerase chain reaction
TEM	Transmission electron microscopy

Hongfei Ge and Xingsen Xue have contributed equally to this work.

✉ Hua Feng
fenghua8888@vip.163.com

✉ Shengli Hu
husl1937@163.com

[1] Department of Neurosurgery and Key Laboratory of Neurotrauma, Southwest Hospital, Third Military Medical University (Army Medical University), Chongqing 400038, People's Republic of China

[2] Department of Neurosurgery, No. 908 Hospital of People's Liberation Army, Nanchang 330000, Jiangxi, People's Republic of China

Introduction

Spinal cord injury (SCI), a devastating neurological impairment, usually occurs in subpopulation with workforce and imposes long-term psychological stress and high

socioeconomic burden for the sufferers, as well as their family [1–3]. Hence, exploring novel strategies for SCI has sparked great interest for researchers. Our previous studies have uncovered a variety of therapeutic candidates associated with secondary injury, including promoting neuron survival through inhibiting acid-sensing ion channel 1a (ASIC 1a) [4] or activating G-protein coupled estrogen receptor 1 (GPER1) [2, 5], mediating neuroinflammation by complement C5a [6], decreasing glial scar formation and potentiating axon regeneration using curcumin, antisense vimentin cDNA combined with chondroitinase ABC [7–9], and cell-based strategies using exogenous transplantation of human umbilical cord mesenchymal stem cells [10], and directing endogenous neural stem cells (NSCs) differentiation into neurons [11, 12]. However, the majority of SCI patients still recover poorly in clinic, implying that more mechanisms need to be elucidated with respect to secondary injury and exploring more effective treatments for SCI is of great significance.

The main research focus for investigators with regard to therapeutic strategies is to promote neuronal regeneration following SCI during the last four decades. While, studies have revealed that 5–10% of the original axons survive during the acute phase of SCI, which would be lost during the chronic stage without appropriate intervention [13–15]. Furthermore, the limited number of epibiotic axons (5–10% of original axons), that wholly or partially execute function during the acute and/or chronic stage of SCI, holds sufficient potential in facilitating locomotor function recovery post-SCI [13–15], suggesting that maximally preserving the function of white matter bundles might be a feasible strategy for SCI treatment.

Oligodendrocyte, a subtype of neural cells, is mainly responsible for myelination in the central nervous system (CNS) [13, 16]. And, previous studies have indicated that oligodendrocyte is susceptible to oxidative damage due to high level of iron deposition induced by hemorrhage in the epicenter of spinal cord after SCI [17–19]. Herein, immediately reducing the iron concentration is supposed to avail oligodendrocyte survival, thereafter, facilitating functional recovery. Coincidently, our previous research has presented that application of deferoxamine (DFX), one of iron chelators, holds the ability of reducing axonal damage and demyelination through downregulation of transferrin receptor and divalent metal transporter 1 (DMT1) to decrease iron overload [20]. Additionally, ferroptosis, a novel form of regulated cell death (RCD) [21], must be triggered due to high level of iron and reactive oxygen species (ROS) accumulation. Most recently, investigators have revealed that iron and ROS accumulation in the motor neurons are evidently increased both in SCI patients and rats to induce ferroptosis in motor neurons, and administration of ferroptosis inhibitor could abolish this harsh situation to accelerate functional recovery, to some extent [22], implying that the administration of ferroptosis inhibitors is a promising therapeutic strategy for SCI.

Ferrostatin-1, the first-generation ferrostatin, is an aromatic amine that perfectly anchors lipid ROS and protects cells against lipid peroxidation [21, 23, 24]. Recent studies have illustrated that ferrostatin-1 bears the ability of scavenging hydroperoxyl radical to reduce cell death through mitigating ferroptosis [24, 25]. Meanwhile, another study has found that ferrostatin-1 bears the potential of suppressing neuroinflammation and ferroptosis resulted from angiotensin Ⅱ in astrocytes in vitro [26], suggesting that ferrostatin-1 exerts multiple protective effects. Additionally, investigations have indicated that ferrostatin-1 protects neural cells from damage through inhibiting ferroptosis in various CNS diseases, such as stroke (ischemic and hemorrhagic subtypes) [27–30], traumatic brain injury (TBI) [28, 31, 32], and neurodegenerative diseases [25, 33, 34], supporting the fact that ferrostatin-1 could penetrate blood–brain barrier (BBB) to exert neuroprotective effect. However, its role and underlying mechanism after SCI are still indefinable.

In the present study, we hypothesized that oligodendrocyte ferroptosis induced by iron and ROS overload played an important role in the secondary white matter injury following SCI, and administration of ferrostatin-1 might reduce oligodendrocyte ferroptosis via reducing iron and ROS deposit, thereafter attenuating white matter injury to promote functional recovery post-SCI in rats. The aim of the present study is to certify the therapeutic effects of ferrostatin-1 on SCI in rats and to offer a possible therapeutic strategy for SCI, even for other CNS diseases existing ferroptosis, from bench to bedside.

Materials and Methods

Animals

All experiments were conducted in accordance with the China's animal welfare legislation for the protection of animals used for scientific purposes. And all procedures were supervised by the Ethics Committee of the Southwest Hospital, Third Military Medical University for the use of laboratory animals (approval no. SYXK 20170002). A total of 126 adult females (200–250 g, 118 rats used for experiments and 8 rats died during experiments) Wistar rats and 50 pregnant Wistar rats were used in the present research. All rats were given free access to food and water under the condition of constant photoperiod (12-h light/dark cycle), temperature (22 °C–25 °C) and moisture (55%–60%) before and after surgery. Every effort was made to reduce the number and to alleviate their sufferings of rats used in the present research.

Surgical Procedures

The surgical procedures were carried out under sterile conditions as previously described [2, 5, 20]. In brief, rats were placed in a stereotaxic frame after anesthesia with 2% isoflurane/air mixture (2–3 l/min). A 4-cm-long incision was introduced in the skin along the midline of the back and a laminectomy was carried out to expose the thoracic 9–11 (T9–11) spinal segments, leaving the dura intact. Thereafter, spinal contusion injury was performed using a 20-g weight rod (diameter 4 mm) dropping from a height of 30 mm onto the exposed T10 segment. Afterward, the muscles and skin were sutured in anatomic layers. Body temperatures were maintained at 37 ± 0.3 °C on a heating pad during surgery. Rats were received manual bladder empty twice a day until they could do themselves and their weight loss, dehydration, autophagia, and discomfort were recorded each day, even with appropriate veterinary care if needed.

Experimental Groups

After surgery, rats were randomly assigned into the following groups:

(i) Sham group. Rats ($n = 10$) were received laminectomy without contusion. Then rats were intraspinally microinjected with the same volume of 0.9% NaCl (containing 0.1% DMSO), equivalently to the volume of ferrostatin-1 in SCI + ferrostatin-1 group, using the same method.
(ii) SCI group. Rats ($n = 15$) were received laminectomy with contusion. Then rats were intraspinally microinjected with the same volume of 0.9% NaCl (containing 0.1% DMSO), equivalently to the volume of ferrostatin-1 in SCI + ferrostatin-1 group.
(iii) SCI + ferrostatin-1 group. Rats ($n = 15$) were received laminectomy with contusion. Four hours after surgery, ferrostatin-1 (0.7 mg/kg, Sigma-Aldrich, Munich, Germany), which was diluted in 0.9% NaCl after dissolved in DMSO, was microinjected into the dorsal spinal cord 2 mm rostrally and 2 mm caudally to the injury site at a depth of 1.2 mm and 0.75 mm laterally from midline at a rate of 1 µl/min. The needle was left in position for a further 2 min before being slowly withdrawn. A total volume of 10 µl Ferrostatin-1 was injected. The second dosage was performed on the second day after SCI.

Behavioral Test

The Basso, Beattie and Bresnahan (BBB) locomotor rating score, a 21-point scale, is widely used to distinguish behavioral outcomes after SCI in rats [35]. The score ranges from 0 to 21, where 0 reflects no locomotor function and 21 indicates normal performance. Rats were allowed to walk around freely in a 90-cm2 field for 5 min, while movements of the hind limb were closely observed. Herein, in the present study, the locomotor recovery of rats in different groups was evaluated using the BBB locomotor rating score by two independent examiners blinded to the experimental groups on days 3, 7, 21, 35, and 56, as previously described [3, 36].

Primary Oligodendrocyte Progenitor Cells (OPCs) Culture

Primary OPCs were isolated from P0–P1 Wistar rats as previously described [37]. Briefly, the spinal cords were collected after rats were euthanized. Then, the dura mater and blood vessels were dissected under a stereomicroscope (SZ61, Olympus, Tokyo, Japan). Subsequently, the samples were triturated using a fire-polished Pasteur pipette and passed with a 40-µm Nylon cell strainer (BD Falcon, San Jose, CA) to collect the dissociated cell suspensions. The cell suspensions were cultured in Dulbecco's modified Eagle's medium (DMEM; Hyclone, Logan, Utah, USA) supplemented with 20% fetal calf serum after centrifugation at 1000 rpm. After 10–12 days, immature oligodendrocytes, attached to the astrocyte layer of the mixed glia culture, were isolated by shaking overnight at 230 rpm. The collected cells were pre-seeded for 30 min at 5% CO_2 and 37 °C to remove contaminating microglia and astrocytes. Floating cells were collected in DMEM supplemented with B27 (Gibco, Grand Island, NY, USA), 10 ng/ml platelet-derived growth factor (PDGF, Peprotech, Rocky Hill, NJ, USA), and 10 ng/ml basic fibroblast growth factor (bFGF, Peprotech, Rocky Hill, NJ, USA) and plated on poly-L-ornithine-coated (Sigma-Aldrich, Munich, Germany) cover slips or culture plates (1×10^5 cells/ml). At this stage the purity of culture was approximately around 95%, assessed by expression of the immature oligodendrocyte surface progenitor markers of Olig2 and O4. Ferrostatin-1 was first dissolved in DMSO and then diluted with culture medium (containing 0.1% DMSO) with the final concentration of 0.5 µM for in vitro experiments. The control or vehicle group was added in the same volume of DMSO as the ferrostatin-1 group.

Perl's Prussian Blue Staining

Rats ($n = 5$) were transcardially perfused with 0.1 M phosphate-buffered saline (PBS), followed by 4% paraformaldehyde (PFA, pH ~ 7.2–7.4) in 0.1 M PBS after anesthesia with 2% isoflurane/air mixture (2–3 l/min) on day 7. The T10 spinal cord segments containing the injury epicenter and surrounding uninjured tissues (6 mm = 3 mm either side from the injury epicenter) were dissected and prepared for paraffin sections according to the standard procedures. Iron accumulation in spinal cords or primary OPCs was determined

using the Perl's Prussian blue staining method, as previously described [20, 38]. Paraffin section (5 μm) from spinal cords was processed through a graded ethanol series, immersed in xylene, and then rehydrated in PBS. Subsequently, samples were immersed in Perls' Staining Solution (comprising equal parts of potassium ferrocyanide and HCL) for 20 min. Afterward, the samples were washed with Milli-Q water and stained with nuclear fast Red for 5–10 min, dehydrated, cleared in xylem, and mounted using a standard procedure. Deposits of iron were stained as blue by Perl's Prussian blue staining, while cytoplasm and cellular nucleus were stained as pink and red, respectively.

Iron Concentration Determination

Spinal cords ($n = 8$) or primary OPCs were collected and homogenized under ice-cold conditions. Iron levels were measured using the tissue iron assay kit (Nanjing Jiancheng Bioengineering Institute, Nanjing, China) in accordance with manufacturer's instruction. To determine iron concentration, the optical density (OD) value was measured at 520 nm using a spectrophotometer (Varioskan Flash, Thermo Scientific, Waltham, MA, USA) and the iron concentration in all samples was then determined through comparing the OD of the samples to the standard curve.

Reactive Oxygen Species (ROS) Measurement

ROS levels were determined by a ROS assay kit according to the manufacturer's specification (cat. no. S0033S, Beyotime Biotechnology, Beijing, China). Spinal cord samples ($n = 3$) or primary OPCs were collected and homogenized under ice-cold conditions. Each sample was loaded 500 μl of 10 μM DCFH-DA and incubated in the dark at 37 °C for 20 min. The loading buffer was replaced and washed three times to eliminate residual DCFH-DA. Thereafter, the samples were immediately measured using a Flow cytometer (ACEA Biosciences Inc., San Diego, CA, USA) with an argon laser (488 nm).

Immunohistochemistry (IHC)

For immunofluorescence staining, slices ($n = 9$) were incubated in 4% paraformaldehyde in 0.01 M PBS for 30 min at room temperature and permeabilized with 0.3% Triton-X 100 (Sigma-Aldrich, St. Louis, MO) in PBS. Then, samples were incubated in the following primary antibodies overnight at 4 °C after blocked with 5% bovine serum album (BSA, Sigma-Aldrich, St. Louis, MO): anti-APP antibody (cat. no. MAB348, Sigma-Aldrich, Munich, Germany), anti-dMBP (cat. no. MBS618031, MyBioSource, San Diego, CA, USA), anti-Olig2 (cat. no. ab109186, Abcam, Cambridge, UK), anti-MBP (cat. no. BA0094, Boster, Wuhan, China), anti-GFAP (cat. no. 13–0300, Thermo Fisher Scientific, Inc., Waltham, MA, USA), anti-Iba-1 (cat. no. 019-19741, Wako, Osaka, Japan), or anti-O4 (cat. no. MAB345, Sigma-Aldrich, Munich, Germany). Sections were then incubated in relative secondary antibodies for 2 h at room temperature. The cell nuclei were counterstained with 4′-6-Diamidino-2-phenylindole (DAPI; Beyotime, Beijing, China) for 10 min at room temperature. Samples were mounted onto glass slides, subsequently images were captured using a confocal microscope (Carl Zeiss, LSM780, Weimar, Germany) and examined by Zen 2011 software (Carl Zeiss, Weimar, Germany).

For immunohistochemistry, slices were de-waxed and antigen-repaired according to the standard procedures [39]. Next, samples were incubated in endogenous peroxidase for 10 min. Sections were incubated in anti-CC1 (cat. no. SAB4501438, Sigma-Aldrich, Munich, Germany) primary antibody overnight at 4 °C after blocked with 5% BSA dissolved in 0.5% v/v Triton-X 100 (Sigma-Aldrich, St. Louis, MO) in PBS. After washing, they were incubated in horseradish peroxidase (HRP)-conjugated goat anti-mouse immunoglobulin G (ZSGB-BIO, Beijing, China). Then, the 3-diaminobenzidine (DAB) kit was employed to stain in color. Sections were counterstained with hematoxylin and dehydrated with ethanol and xylene to prep for mounting. Thereafter, coverslips were mounted onto glass slides. Images were captured using a light microscope (Olympus, Tokyo, Japan).

For each sample, six sections were immunostained, analyzed, calculated, and reported as the average of four independent measurements. All measurements were performed by an individual investigator who was blinded to the experiment groups.

Western Blot

The T10 spinal cord segments ($n = 3$) containing the injury epicenter and surrounding uninjured tissues (0.5 cm = 0.25 cm either side from the injury epicenter) were immediately dissected after decapitation post-SCI on day 7. The tissue lysates were collected, and the protein concentration of each sample was determined using a Bicinchoninic Acid (BCA) method (Beyotime, Beijing, China). Proteins (50 μg) were separated by 10% SDS-PAGE under reducing conditions and electro-blotted to polyvinylidene difluoride (PVDF, Roche, Indianapolis, IN, USA) membranes. Then, the membranes were incubated in 5% (w/v) non-fat dry milk (Beyotime Institute of Biotechnology) in TBS with Tween-20 (TBST) at room temperature for 2 h. Thereafter, the membranes were cut out at different parts according to a pre-stained protein molecular ladder (cat. no. 26616; Thermo Fisher Scientific, Inc., Waltham, MA, USA) to allow separate detection of proteins migrating at the same distance and were incubated in primary antibodies, anti-APP antibody (cat. no. MAB348, Sigma-Aldrich, Munich, Germany),

anti-dMBP (cat. no. MBS618031, MyBioSource, San Diego, CA, USA), anti-IREB2 antibody (cat. no. SAB2501280, Sigma-Aldrich, Munich, Germany), anti-PTGS2 (cat. no. ab179800, Abcam, Cambridge, UK), or anti-GAPDH (cat. no. AF0006; Beyotime Institute of Biotechnology) overnight at 4 °C. Afterward, the membrane was incubated in corresponding horseradish peroxidase (HRP)-conjugated secondary antibody after rinsed twice with TBST. All membranes were visualized by a ChemiDoc™ XRS+ imaging system (Bio-Rad, California, USA) using the WesternBright ECL Kits (Advansta, Menlo Park, CA, USA). Densitometric measurement of each membrane was performed using Image Lab™ software (Bio-Rad, California, USA).

Reverse Transcription-Quantitative Polymerase Chain Reaction (RT-qPCR)

Total RNA was extracted using a TaKaRa MiniBEST Universal RNA Extraction Kit (TaKaRa, Tokyo, Japan) according to the manufacturer's instructions after primary OPCs were collected from each group. Thereafter, 1 μg RNA was reversely transcribed into cDNA using a PrimeScript RT reagent Kit with gDNA Eraser (cat. no. RR0047A, TaKaRa, Tokyo, Japan) according to the manufacturer's direction. Subsequently, qPCR was performed using the CFX96 System (Bio-Rad, CA, USA) with SYBR Premix Ex TaqII (Tli RNaseH Plus) (cat. no. RR820A, TaKaRa, Tokyo, Japan) under the following conditions: 95 °C for 30 s, 40 cycles at 95 °C for 5 s, and 60 °C for 30 s. Relative mRNA levels were normalized to GAPDH and analyzed using the $2^{-\Delta\Delta Cq}$ method. Primer sequences used in the present study were as follows:

Primer	Forward	Reverse
IREB2	5′-GAGACTGGGCTG CGAAAGGA-3′	5′-CCTGGGAGGAACTCA AGTGGTG-3′
PTGS2	5′-TCACCCGAGGACTGG GCCAT-3′	5′-TGGGAGGATACACCT CTCCACCG-3′
GAPDH	5′-AACCTGCCAAGTATG ATGACATCA-3′	5′-TGTTGAAGTCACAGG AGACAACCT-3″

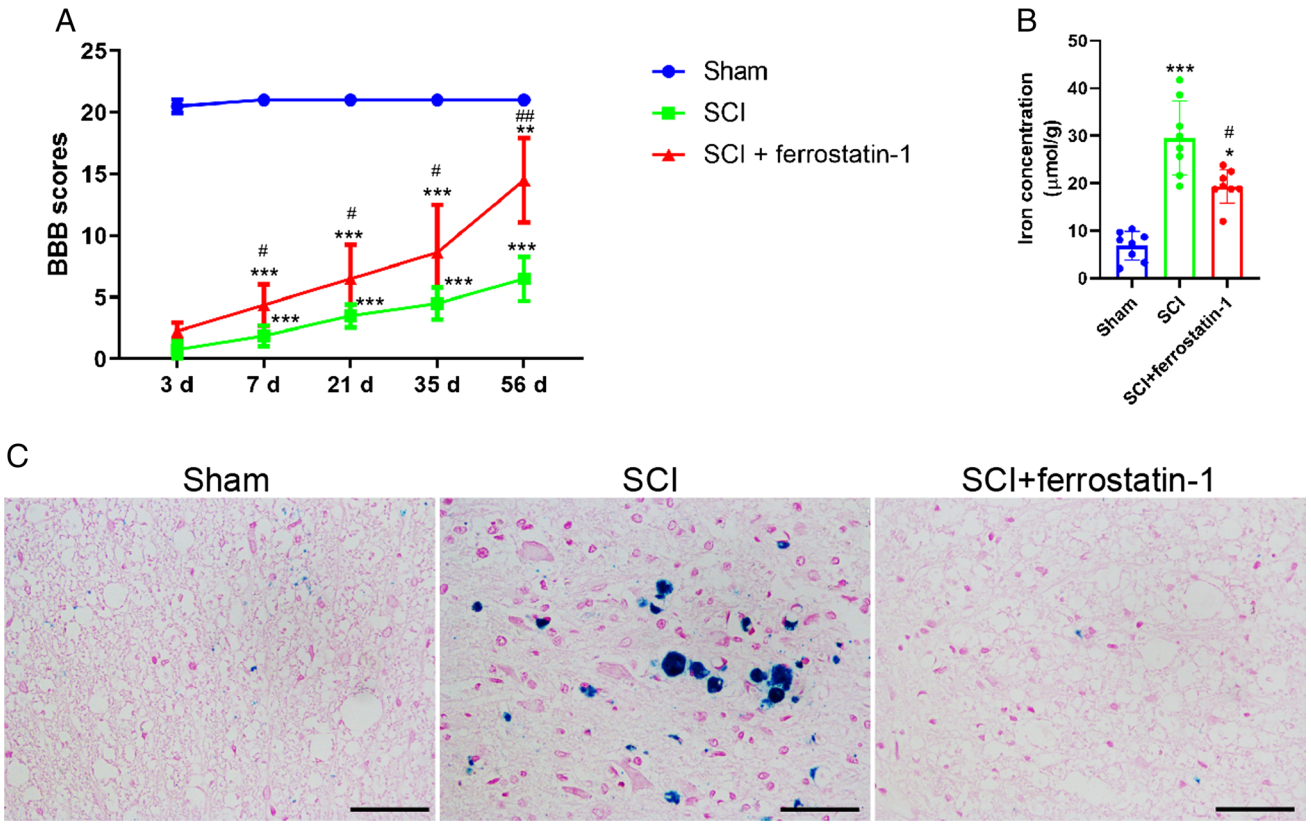

Fig. 1 Ferrostatin-1 promotes functional recovery through reducing iron deposition in rats after spinal cord injury (SCI). **A** Summarized data showing the post-injury motor behavior using Basso, Beattie and Bresnahan (BBB) score in different groups on day 3, 7, 21, 35, and 56 post-SCI. ***$P < 0.01$ vs. Sham; **$P < 0.01$ vs. Sham; #$P < 0.05$, ##$P < 0.01$ vs. SCI. **B** The iron concentration in the epicenter of injured spinal cord on day 7 in different groups. **C** Perl's Prussian blue staining images showing the iron accumulation in the epicenter of injured spinal cord on day 7 in different groups. Scale bar: 50 μm

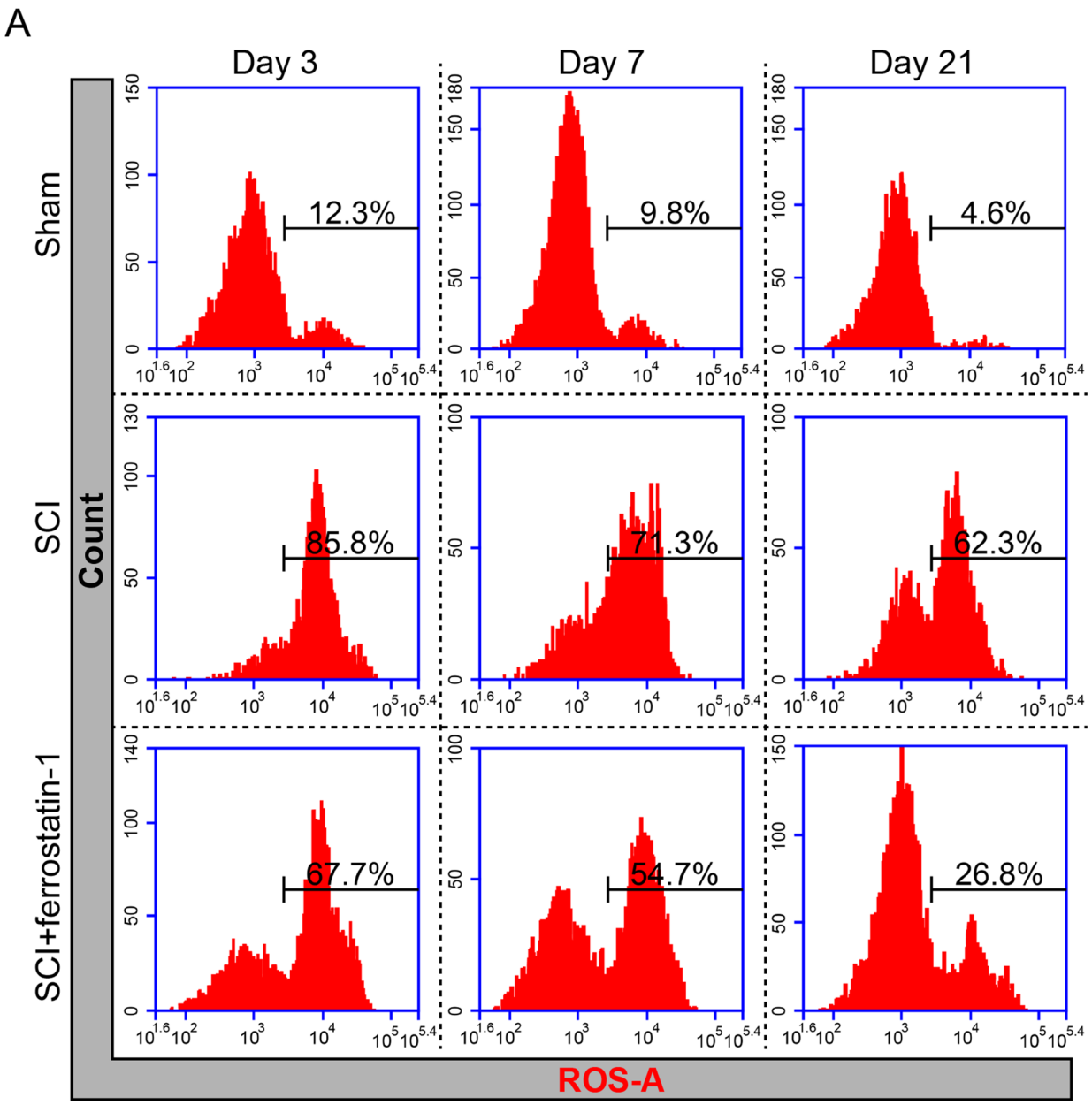
A
Day 3
Day 7
Day 21
Sham
SCI
SCI+ferrostatin-1
Count
ROS-A
12.3%
9.8%
4.6%
85.8%
71.3%
62.3%
67.7%
54.7%
26.8%

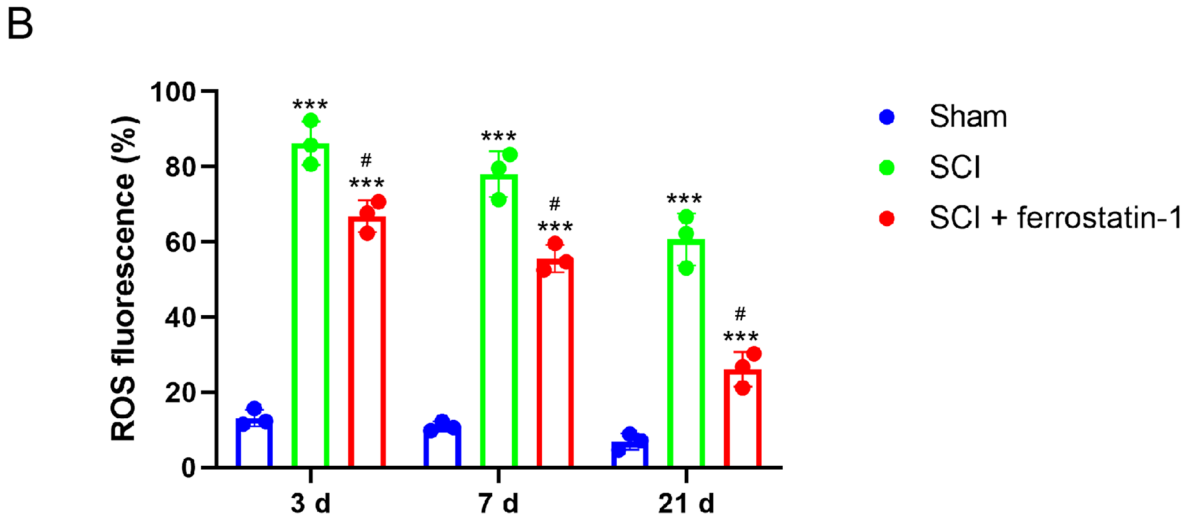
B
ROS fluorescence (%)
3 d
7 d
21 d
Sham
SCI
SCI + ferrostatin-1

◂**Fig. 2** Ferrostatin-1 reduces reactive oxygen species (ROS) accumulation in the epicenter post-SCI. **A** Representational images indicating the ROS accumulation using Flow Cytometry. **B** Bar graph summarizing the percentage of ROS fluorescence from (**A**). ***$P < 0.01$ vs. Sham; #$P < 0.05$, ##$P < 0.01$ vs. SCI

Transmission Electron Microscopy (TEM)

TEM was performed to visualize ultrastructure of primary OPCs in different groups, as previously described [39]. Primary OPCs from each group were incubated in 2% glutaraldehyde overnight at 4 °C and then

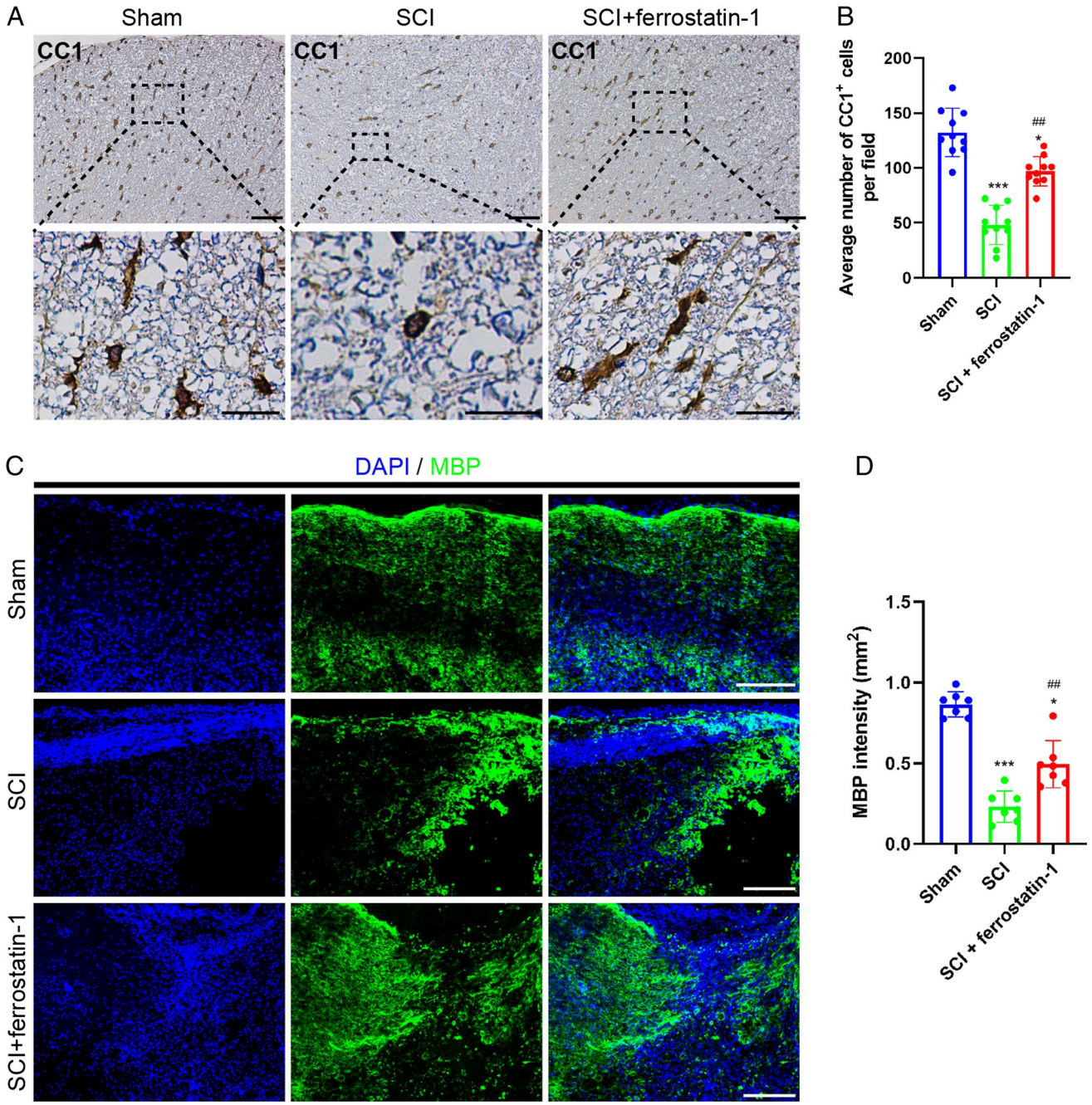

Fig. 3 Ferrostatin-1 facilitates myelination post-SCI on day 7. **A** Representative immunohistochemistry images of CC1 in the epicenter of injured spinal cord on day 7 in different groups. Scale bar: 50 μm; 10 μm for enlarged images. **B** Bar chart indicating the average number of $CC1^+$ cells per field (200×). ***$P < 0.01$, *$P < 0.05$ vs. Sham; ##$P < 0.01$ vs. SCI. **C** Immunostaining depicting the expression of in each group. Scale bar: 100 μm. **D** Semi-quantitative data showing the optic density of MBP in each group. ***$P < 0.01$, *$P < 0.05$ vs. Sham; ##$P < 0.01$ vs. SCI

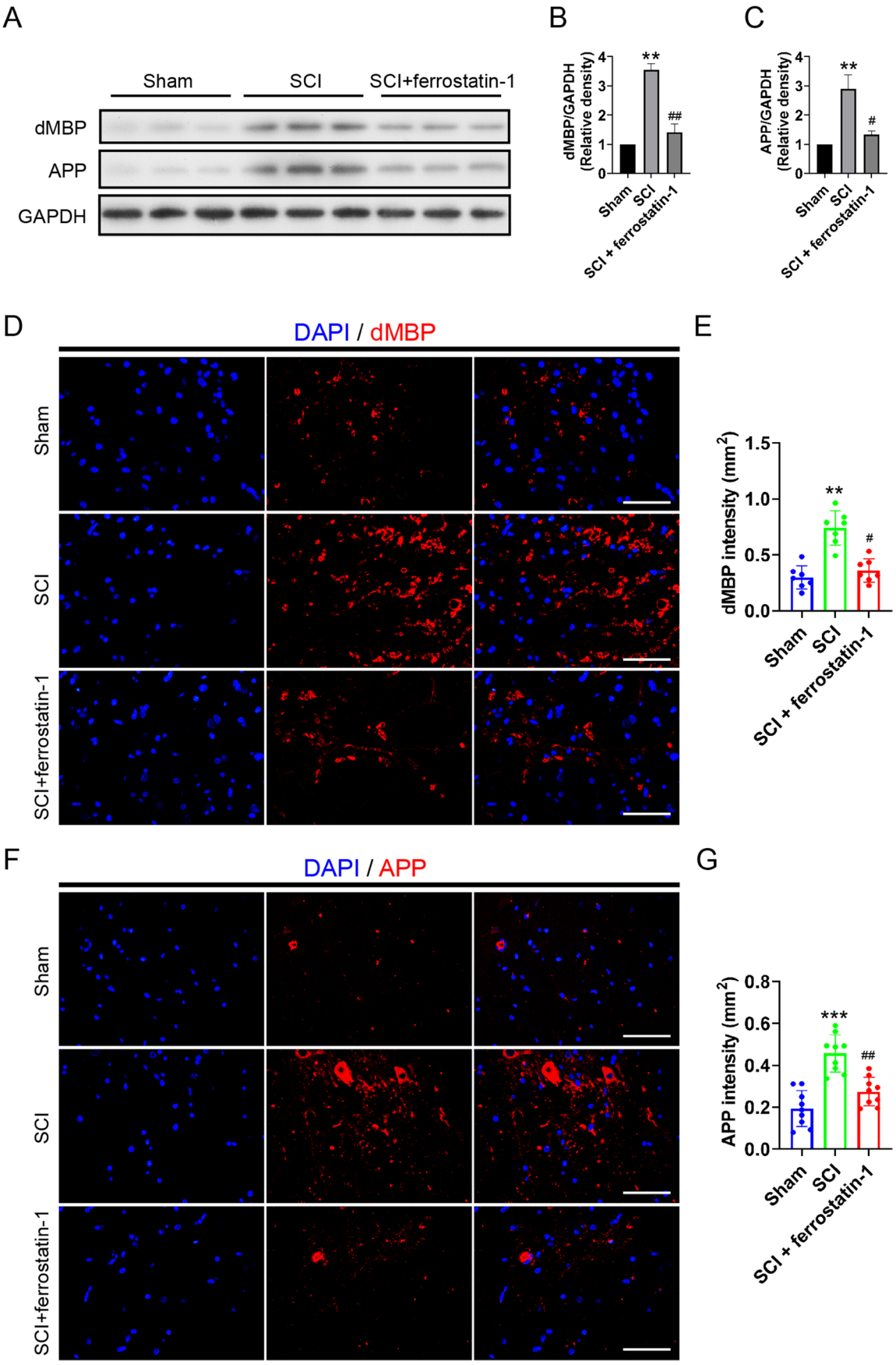
A
Sham
SCI
SCI+ferrostatin-1
dMBP
APP
GAPDH
B
dMBP/GAPDH (Relative density)
**
##
Sham
SCI
SCI + ferrostatin-1
C
APP/GAPDH (Relative density)
**
#
Sham
SCI
SCI + ferrostatin-1
D
DAPI / dMBP
Sham
SCI
SCI+ferrostatin-1
E
dMBP intensity (mm²)
**
#
Sham
SCI
SCI + ferrostatin-1
F
DAPI / APP
Sham
SCI
SCI+ferrostatin-1
G
APP intensity (mm²)
***
##
Sham
SCI
SCI + ferrostatin-1

◂**Fig. 4** Ferrostatin-1 decreases demyelination post-SCI on day 7. **A** Immunoblot bands representing the expression level of dMBP and APP in various groups. GAPDH was served as an internal control. **B, C** Semi-quantitative analysis of the expression of dMBP **B** and APP **C** from **A**. $^{**}P < 0.01$ vs. Sham; $^{\#}P < 0.05$, $^{\#\#}P < 0.01$ vs. SCI. **D** Immunostaining images delineating the expression of dMBP in each group. Nuclei were counterstained with DAPI. Scale bar: 20 μm. **E** Semi-quantitative data showing the optic density of dMBP in each group. $^{**}P < 0.01$ vs. Sham; $^{\#}P < 0.05$ vs. SCI. **F** Immunostaining images demonstrating the expression of APP in different groups. Scale bar: 20 μm. **G** Semi-quantitative bar graph indicating the optic density of APP in each group. $^{***}P < 0.001$ vs. Sham; $^{\#\#}P < 0.01$ vs. SCI

transferred to 1% citric acid for fixation. Thereafter, they were dehydrated with gradient acetone after soaking in uranyl acetate. Subsequently, samples were embedded with epoxy resin and sliced into 70–90 nm. Then, they were counterstained with lead citrate after placing on the copper trough grid and the ultrastructure of mitochondria was observed using a transmission electron microscope (Hitachi HT7700, Tokyo, Japan). At least three independent samples per group were used for TEM analysis.

Statistical Analysis

Statistical analysis was performed using Graphpad version 9.0 (Graphpad Software Inc., San Diego, CA, USA). Comparisons between two groups were analyzed using analysis of variance (ANOVA), followed by Tukey's post hoc test in case of the data were normality using a Shapiro–Wilk normality test. Meanwhile, data failing the normality test were represented as median and interquartile range (IQR) using the Mann–Whitney *U* test. A $P < 0.05$ was considered as significant difference.

Results

Ferrostatin-1 Improved Motor Behavior Through Decreasing Iron and ROS Accumulation in Rats after SCI

To evaluate the effect of ferrostatin-1 on functional recovery after SCI, the BBB score was firstly performed. The results indicated that the BBB score of rats in SCI + ferrostatin-1 group was evidently higher than that in SCI group from day 7 to 56 (Fig. 1A). Given that ferrostatin-1 is an inhibitor of ferroptosis and iron is the main trigger of ferroptosis, we then determined the iron concentration. The results showed that ferrostatin-1 significantly reduced the iron concentration, whose level was greatly elevated in spinal cords after SCI (Fig. 1B). Next, the Perl's Prussian blue staining was conducted to verify the iron deposition in the epicenter of injured spinal cords. The images delineated that ferrostatin-1 dramatically reduced the iron accumulation in the epicenter of injured spinal cords (Fig. 1C). With respect to the high level of iron could directly or indirectly upregulate the ROS accumulation after injury [40], we thereafter determined the level of ROS in the epicenter of damaged spinal cords. The results indicated that ferrostatin-1 predominantly reduced the ROS fluorescence, which was substantially increased in the injured spinal cords, on days 3, 7, and 21 (Fig. 2A, B). Collectively, these results illustrated that ferrostatin-1 facilitated locomoter deficits via deducing iron and ROS accumulation post-SCI in rats.

Ferrostatin-1 Enhanced Myelination and Attenuated White Matter Injury after SCI in rats

Given that oligodendrocytes are susceptible to oxidative damage and high level of iron deposition after SCI [17–19], the average number of oligodendrocytes was firstly evaluated using immunochemistry. The results depicted that the number of $CC1^+$, which is usually used to specifically label mature oligodendrocytes [41], was dramatically deduced in the epicenter of spinal cords after SCI (Fig. 3A, B), while ferrostatin-1 partially abrogated this effect, that was administration of ferrostatin reduced oligodendrocytes loss (Fig. 3A, B). Meanwhile, the expression of Myelin Basic Protein (MBP), which is responsible for adhesion of the cytosolic surfaces of multilayered compact myelin [42], was elucidated using immunostaining. The results substantiated that the expression of MBP was obviously downregulated, while administration of ferrostatin-1 partially abrogated this inhibitory effect (Fig. 3C, D. Next, the expression of degraded myelin basic protein (dMBP), a symbol of myelin degradation, and APP-a maker of damaged axons, was determined using western blot assays. The bands depicted that the expression of dMBP and APP was substantially elevated surrounding the epicenter of spinal cord after SCI in rats (Fig. 4A–C). However, the enhanced expression of dMBP and APP was obviously downregulated with ferrostatin-1 treatment (Fig. 4A–C). Moreover, the immunostaining images represented that ferrostatin-1 evidently decreased the optic intensity of dMBP that was upregulated post-SCI (Fig. 4D, E). Subsequently, the immunostaining of APP showed the similar phenomenon as dMBP and further attested the results obtained from western blot assays (Fig. 4F, G). Mechanically, these results suggested that ferrostatin-1 held the ability of promoting myelination and attenuating demyelination via reducing the oligodendrocytes loss after SCI.

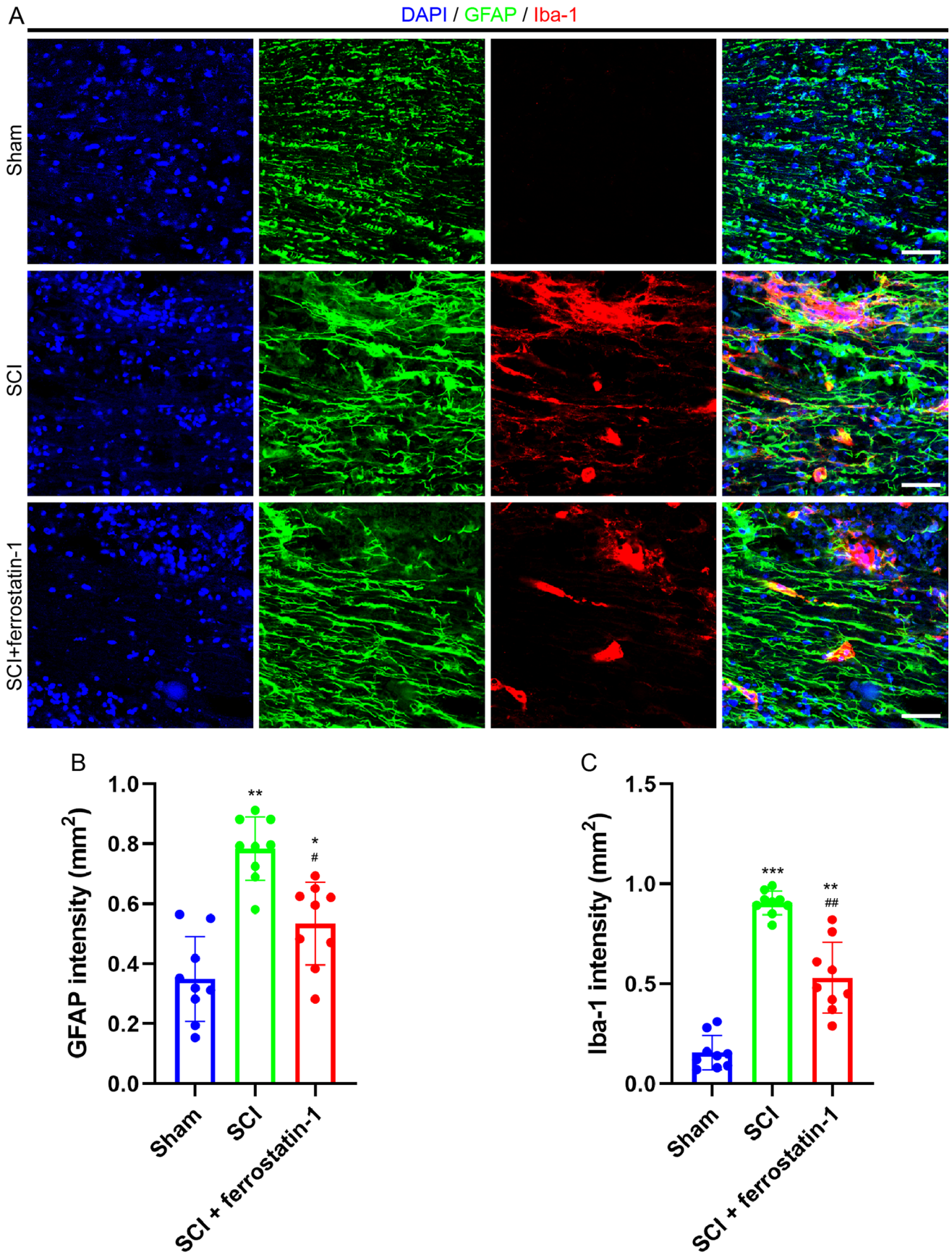
A
DAPI / GFAP / Iba-1
Sham
SCI
SCI+ferrostatin-1
B
GFAP intensity (mm2)
1.0
0.8
0.6
0.4
0.2
0.0
**
*
#
Sham
SCI
SCI + ferrostatin-1
C
Iba-1 intensity (mm2)
1.5
1.0
0.5
0.0
***
**
##
Sham
SCI
SCI + ferrostatin-1

◂**Fig. 5** Ferrostatin-1 inhibits the activation of reactive astrocyte and microglia post-SCI on day 7. **A** Immunostaining images representing the expression of GFAP and Iba-1 in each group. Nuclei were counterstained with DAPI. Scale bar: 50 μm. **B** Semi-quantitative bar chart showing the optic density of GFAP in each group. $*P<0.05$, $**P<0.01$ vs. Sham; $\#P<0.05$ vs. SCI. **C** Semi-quantitative bar graph indicating the optic density of APP in each group. $**P<0.01$, $***P<0.001$ vs. Sham; $\#\#P<0.01$ vs. SCI

Ferrostatin-1 Inhibits the Activation of Reactive Astrocyte and Microglia Post-SCI in Rats

Given that ferrostatin-1 bears the capacity of suppressing activation of reactive astrocytes and inhibiting neuroinflammation through attenuating microglia activation [26, 43], the expression of GFAP and Iba-1 was assessed using immunostaining. The results represented that the expression of GFAP was prominently increased in the epicenter of spinal cord (Fig. 5A, B), while this enhanced effect was dramatically abrogated with administration of ferrostatin-1 (Fig. 5A, B). Meanwhile, the configuration of $GFAP^+$ cells in group SCI + ferrostatin-1 was more regular than that in group SCI (Fig. 5A). Additionally, the number of activated microglia was remarkably reduced with ferrostatin-1 application (Fig. 5A, C). Collectively, these results revealed that ferrostatin-1 possessed the potential of curbing the activation of reactive astrocyte and microglia in the epicenter of spinal cord post-SCI in rats.

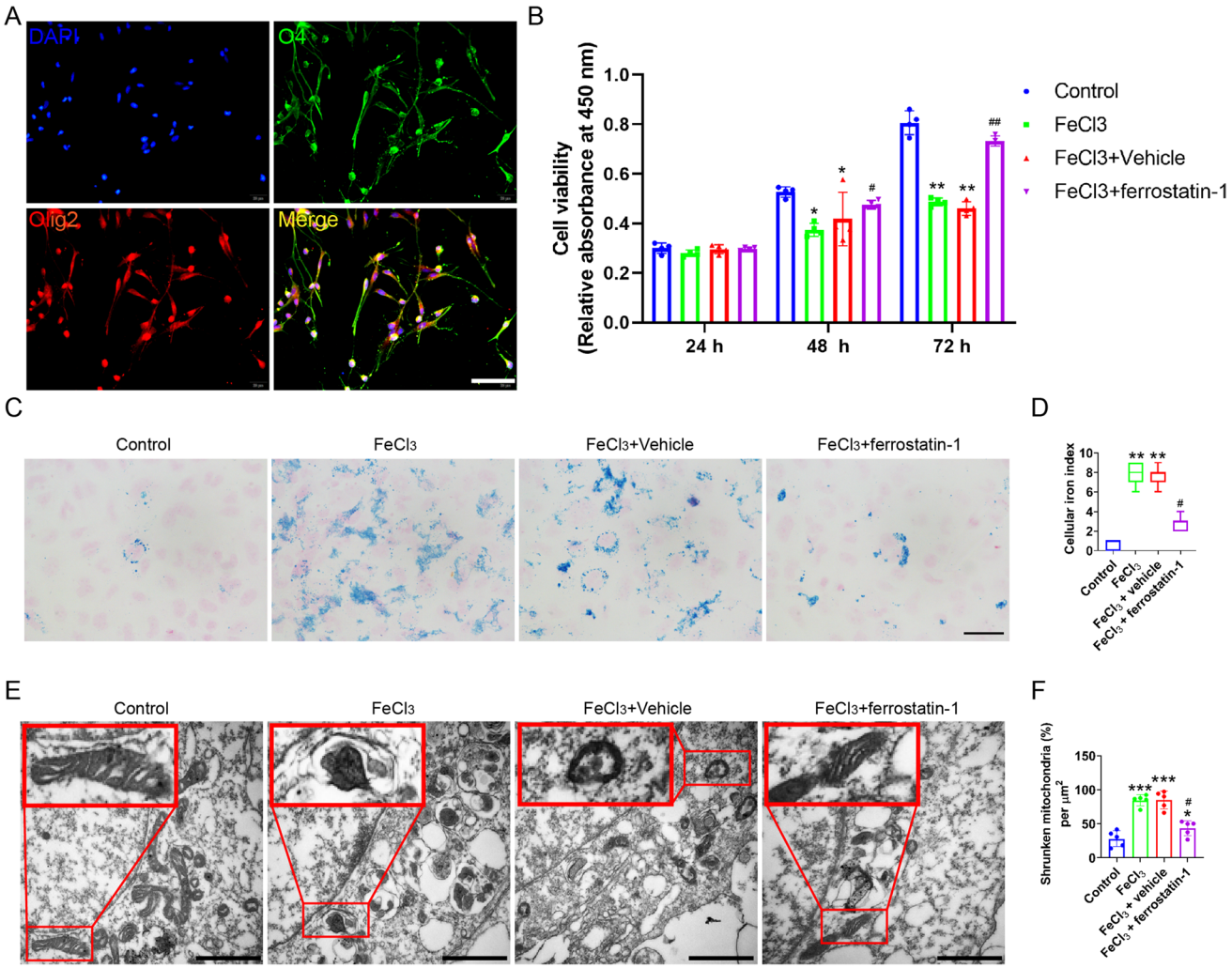

Fig. 6 Ferrostatin-1 reduces OPCs injury induced by iron overload through reducing ferroptosis in vitro. **A** Representative immunostaining images of O4 (green) and Olig2 (red) in primary OPCs. Nuclei were counterstained with DAPI. Scale bar: 20 μm. **B** Bar chart showing cell viability determined by CCK8 in each group at different time points. $*P<0.05$, $**P<0.01$ vs. Control; $\#P<0.05$, $\#\#P<0.01$ vs. $FeCl_3$ or $FeCl_3$ + Vehicle. **C** Perl's Prussian blue staining images showing the iron accumulation in primary oligodendrocytes at 48 h in different groups. Scale bar: 50 μm. **D** Summarized data indicating cellular iron index from (**C**). $**P<0.01$ vs. Control; $\#P<0.05$ vs. $FeCl_3$ or $FeCl_3$ + Vehicle. **E** Transmission electron microscopy of primary oligodendrocytes at 48 h in each group. Scale bars: 1 μm. **F** Quantitation of the shrunken mitochondria per μm^2 in each group. $***P<0.001$, $*P<0.05$ vs. Control; $\#P<0.05$ vs. $FeCl_3$ or $FeCl_3$ + Vehicle

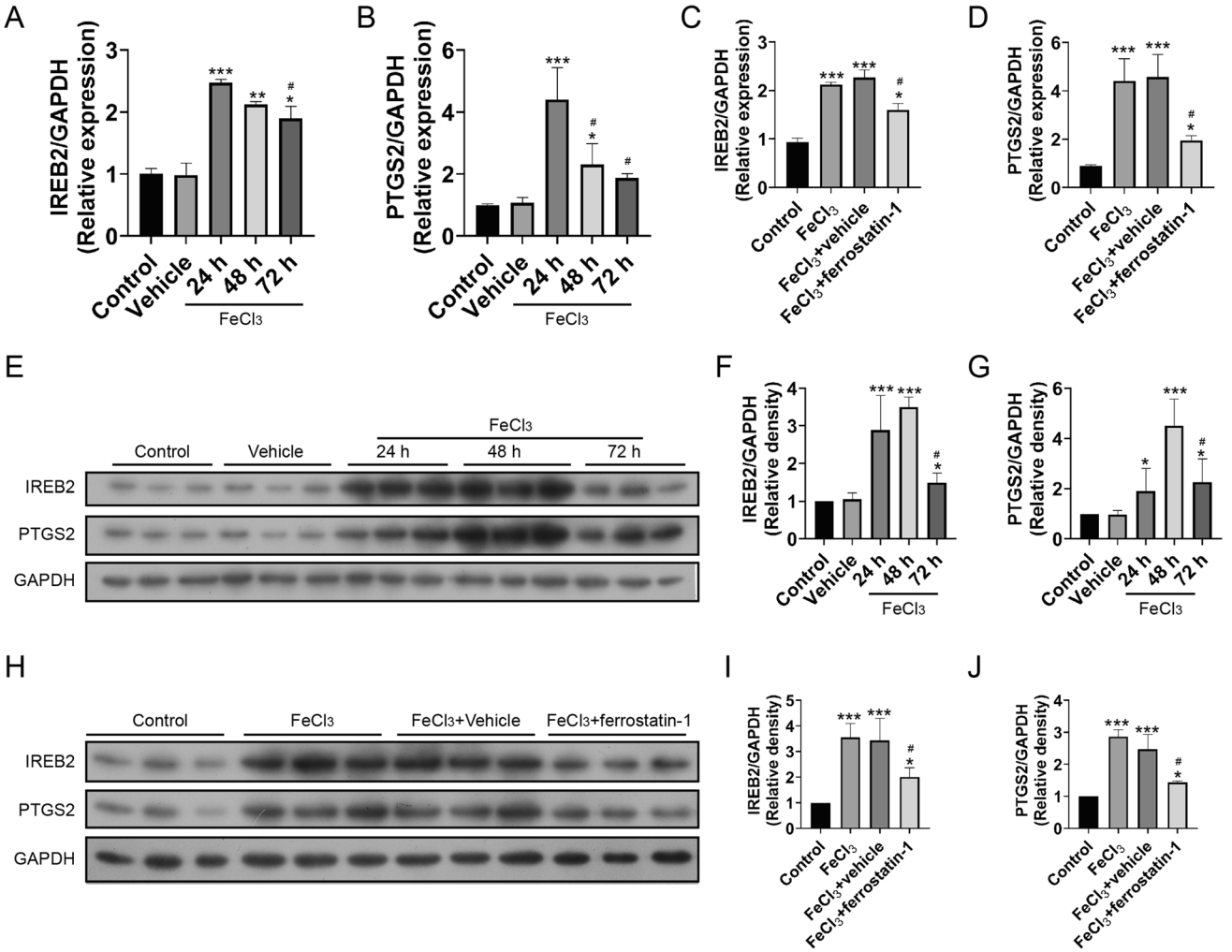

Fig. 7 Ferrostatin-1 alleviates OPCs ferroptosis resulting from iron overload through decreasing IREB2 expression. **A, B** IREB2 (**A**) and PTGS2 (**B**) mRNA expression evaluated by RT-qPCR in each group at different time points. $***P<0.001$, $**P<0.01$, $*P<0.05$ vs. Control or Vehicle; $\#P<0.05$ vs. $FeCl_3$ at 24 h or 48 h. **C, D** IREB2 (**C**) and PTGS2 (**D**) mRNA expression evaluated by RT-qPCR with ferrostatin-1 administration at 48 h in each group. $***P<0.001$, $*P<0.05$ vs. Control; $\#P<0.05$ vs. $FeCl_3$ or $FeCl_3$ + Vehicle. **E** Immunoblot bands representing the expression level of IREB2 and PTGS2 in each group at different time points. GAPDH was served as an internal control. **F, G** Semi-quantitative analysis of the expression of IREB2 (**F**) and PTGS2 (**G**) from (**E**). $***P<0.001$, $*P<0.05$ vs. Control or Vehicle; $\#P<0.05$ vs. $FeCl_3$ at 24 h or 48 h. **H** Immunoblot bands indicating the expression level of IREB2 and PTGS2 at 48 h in each group. GAPDH was served as an internal control. **I, J** Semi-quantitative analysis of the expression of IREB2 (**I**) and PTGS2 (**J**) from (**H**). $***P<0.001$, $*P<0.05$ vs. Control; $\#P<0.05$ vs. FeCl3 or FeCl3 + Vehicle

Ferrostatin-1 Facilitated Oligodendrocyte Progenitor Cells (OPCs) Survival Through Decreasing Ferroptosis In vitro

To further unravel the underlying mechanism that ferrostatin-1 enhanced oligodendrocytes survival in vivo, the primary OPCs were isolated from P0–P1 Wistar rats. As shown in Fig. 6A, most of the cultured cells expressed Olig2 and O4 and exhibited the morphology of OPCs. Considering that the iron concentration was about 30 μM/g in the epicenter of injured spinal cords (Fig. 1B), 20 μM $FeCl_3$ was then used to mimic the iron concentration in *ex vivo* experiments. The results showed that 20 μM $FeCl_3$ greatly reduced OPCs viability from 48 to 72 h and this deduced viability could be partially reversed with addition of 0.5 μM ferrostatin-1 (Fig. 4B). Thereafter, the iron deposition in primary OPCs was evaluated using Perl's Prussian blue staining at 48 h. The results demonstrated that the cellular iron index was significantly upregulated with 20 μM $FeCl_3$ in groups $FeCl_3$ and $FeCl_3$ + vehicle (Fig. 6C, D). However, this effect was prevalently abolished with addition of 0.5 μM ferrostatin-1, in a degree (Fig. 6C, D). In addition, the TEM was conducted to observe the morphology of mitochondria and the results showed that the proportion of shrunken mitochondria was

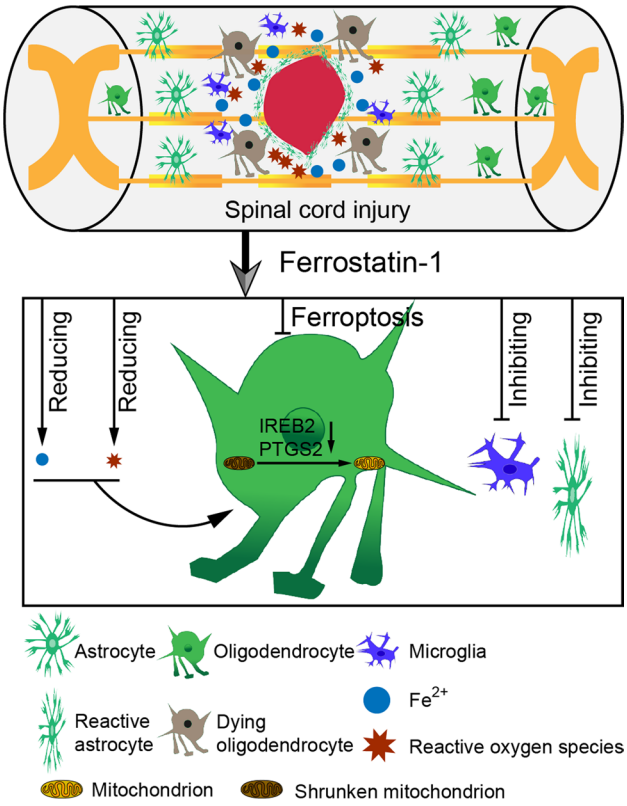

Fig. 8 Schematic illustration for the potential therapeutic effects of ferrostatin-1 on SCI and the underlying mechanism

markedly increased in groups of $FeCl_3$ and $FeCl_3$ + vehicle (Fig. 6E, F), while addition of 0.5 μM ferrostatin-1 abolished this phenomenon, to some extent (Fig. 6E, F). In sum, these results illustrated that ferrostatin-1 bores the potentiality of reducing iron and ROS deposition in OPCs to decrease ferroptosis resulting from iron overload in vitro.

Ferrostatin-1 Mitigated OPCs Ferroptosis Resulting from Iron Overload Through Reducing IREB2 Expression

With respect to ferrostatin-1 potentiates hydroperoxyl radical scavenging to reduce ferroptosis [24, 25] and reduce iron overload in neurons after traumatic brain injury (TBI) [31], we then tested the effect of ferrostatin-1 on OPCs ferroptosis in vitro. First, the RT-qPCR assays indicated that the expression of IREB2 and PTGS2 mRNA was significantly increased from 24 to 72 h (Fig. 7A, B). Then, ferrostatin-1 was used to investigate its role in the expression of IREB2 and PTGS2 mRNA. The results represented that ferrostatin-1 partially decreased the expression of IREB2 and PTGS2 mRNA, which was predominantly elevated with $FeCl_3$ addition at 48 h (Fig. 7C, D). Thereafter, the western blot assays were performed to certify the results obtained from RT-qPCR. The results indicated that the expression of IREB2 and PTGS2 was dramatically increased with $FeCl_3$ addition from 24 to 72 h and both of IREB2 and PTGS2 reached the peak at 48 h (Fig. 7E–G). Subsequently, ferrostatin-1 was added to determine its role in attenuating ferroptosis induced by $FeCl_3$. The results displayed that ferrostatin-1 deduced the expression of IREB2 and PTGS2 at 48 h (Fig. 5H–J). Mechanically, these results represented that iron accumulation resulted in upregulation of ferroptosis-related genes and proteins, as well as increase of shrunken mitochondria, while ferrostatin-1 eliminated this effect, to some extent.

Discussion

The present study provides evidence that iron and ROS accumulation occur in the epicenter of spinal cord after SCI, which may lead to severe white matter injury and locomotor function deficits. Iron overload induces ROS production, subsequently initiating oligodendrocytes ferroptosis. Moreover, administration of ferrostatin-1, one specific inhibitor of ferroptosis, exerts versatile functions, including but not limited to reducing the content of iron and ROS to alleviate oligodendrocytes ferroptosis, inhibiting activation of astrocyte and microglia, thereafter promoting neurological functional recovery due to attenuating white matter damage in rats subjected to SCI (Fig. 8). These data indicate that ferroptosis elicited by iron overload plays an important role in the secondary white matter injury post-SCI.

It is generally believed white matter injury to be a potential role in neurological loss after SCI. In recent years, more and more attention has been paid to white matter repair after SCI, which is considered to be a key factor for functional recovery post-SCI. Obtained evidence shows that white matter damage induced by SCI not only occurs in the epicenter of the damaged site but also extends beyond a few millimeters, within minutes to days [13]. Thereafter, oligodendrocyte loss usually peaks at 7 days and persists for up to 2 weeks after injury [44, 45], which is in line with our previous study that severe white matter injury presents after SCI in rats [20]. Our previous study shows that remarkable iron deposition has been observed in spinal cord after SCI, which activates the iron transport system, enhances the expression of DMT1 and transferrin receptor (TfR), then results in intracellular iron overload, accompanied by white matter injury [20]. Deferoxamine (DFX), one of the iron chelators, could reduce iron accumulation and lessen white matter damage, which indicates that iron overload contributes to white matter injury post-SCI [20]. These researches address a question: how does iron accumulation trigger the prolonged white matter injury resulting from oligodendrocytes loss?

Ferroptosis, a new form of cell death [21] that is intrinsically linked to iron overload, offers an answer to the above question. Iron overload not only induces ferroptosis but also results in ROS surplus and vice versa [46]. This positive loop exaggerates oligodendrocyte loss after SCI. Hence, reducing iron overload is a central link to interrupt this vicious paradigm and provides a therapeutic target for SCI. Here, our results proved that the administration of ferrostatin-1 reduced iron and ROS deposition, and then introducing white matter ferroptosis in vitro and in vivo, which is supported by previous study that ferrostatin-1 protects neuronal loss through downregulation of ferroptosis after TBI [31]. Moreover, ferrostatin-1 might also facilitate astrocytes preservation through blocking angiotensin Ⅱ to alleviate neuroinflammation and ferroptosis [26]. Overall, ferroptosis is a central link between various pathological processes, and ferrostatin-1 could interrupt this vicious circle to rehabilitate local neuro-network after SCI. These results enlarge the scope of ferrostatin-1 in treating SCI.

Ferroptosis is a common pathological process in diverse CNS diseases including stroke (ischemic and hemorrhagic subtypes) [27–30], traumatic brain injury (TBI) [28, 31, 32], and neurodegenerative diseases [25, 33, 34]. In the present study, our results provided convincing evidence that ferroptosis played an evident role in oligodendrocytes damage after SCI. Oligodendrocyte, which is responsible for myelination in the CNS, assists neurons to exert better function. While demyelination, which usually retards rapid nerve conduction, is a common phenomenon after SCI. Furthermore, previous studies have represented that reinforcing remyelination during the acute phase of SCI is a beneficial strategy to protect denuded axons from degeneration and to maintain neurological functions that would be lost during the chronic stage [13]. Thus, the present study offers a new insight into the mechanism of white matter injury post-SCI.

The neuroprotective effects of ferroptosis inhibitors on CNS diseases must be multifaced. Our results indicated that ferrostatin-1 could inhibit activation of reactive astrocyte and microglia, which is consistent with previous study that liproxstatin-1, one of another ferroptosis inhibitors, represses activation of reactive astrocyte and microglia through suppressing ferroptosis in rats with peripheral nerve injury [43], suggesting that other ferroptosis inhibitors might be beneficial for SCI such as Epigallocatechin-3-gallate (EGCG) [47] and Zinc [48]. Furthermore, a recent research has represented that iron and ROS accumulation in the motor neurons are certified both in SCI patients and rats to induce ferroptosis in motor neurons, and administration of ferroptosis inhibitor could abolish this harsh situation to accelerate functional recovery, in a degree [22]. Together, these evidence show several neural subtypes (including neurons, microglia, and astrocyte) suffer from ferroptosis and ferroptosis inhibitors exert neuroprotective effects on these neural subtypes.

Several limitations need to be clarified in our future research. First, to decipher the further signaling pathways underlying neuroprotective effect of ferrostatin-1, some protein expression with respect to ferroptosis, such as glutathione (GSH), glutathione peroxidase 4 (GPX4), nuclear factor E2 (NFR2), and ferroptosis suppressor protein 1 (FSP1), needs to be determined. Next, previous report indicates that p53 upregulation induces ferroptosis in cerebral ischemic penumbra [27]. Meanwhile, TLR4/NF-kB axis is associated with inflammation and oxidative stress to initiate ferroptosis [49]. Given that ferrostatin-1 is an anti-ferroptosis agents, whether ferrostatin-1 could downregulate the expression of p53 and/or reduce the activity of TLR4/NF-kB axis, should be elucidated. In addition, several cell death pathways are activated when ROS accumulation including apoptosis, autophagy, ferroptosis, and necrosis. Whether a crosstalk exist among these cell death pathways and which molecule is the trigger are of worthy investigating.

Conclusion

In conclusion, this study reveals the novel findings that ferroptosis plays a distinct role in the secondary white matter injury, and ferrostatin-1 reduces iron and ROS accumulation and downregulates the ferroptosis-related genes and its products of IREB2 and PTGS2 to further inhibit ferroptosis in oligodendrocyte, finally reducing white matter injury and promoting functional recovery following SCI in rats. Meanwhile, ferrostatin-1 holds the potential of inhibiting the activation of reactive astrocyte and microglia. Mechanically, the present study enlarges the therapeutic effects of ferrostatin-1 on SCI and even in other central nervous system (CNS) diseases existing ferroptosis.

Acknowledgements Not applicable.

Author contributions HFG and XSX performed most of the experiments, with assistance from JSX, LBY, YJZ, JZ, JTS, LW, ZYJ, HS, and TNC. HFG and XSX analyzed the results and edited figures. JSX, YJZ, ZYJ, and JZ performed SCI model and statistical analysis. HFG and LW performed cell culture and treatments. HFG, JTS, JW, and TNC performed immunoblotting and immunostaining. HFG wrote preliminary draft of the manuscript. SLH and HF designed experiments and revised the manuscript. All authors approved final version of the manuscript.

Funding This work was supported by grants from the National Natural Science Foundation of China (approval no. 81471261) and Natural Science Foundation of Chongqing (approval no. cstc2018jcyjAX0080).

Data Availability The data that support the findings of this study are available from the corresponding author upon reasonable request.

Declarations

Conflict of interest The authors have no relevant financial or non-financial interests to disclose.

Informed Consent Not applicable.

Research Involving Human and Animals Participants All experiments were conducted in accordance with the China's animal welfare legislation for the protection of animals used for scientific purposes. And all procedures were supervised by the Ethics Committee of the Southwest Hospital, Third Military Medical University for the use of laboratory animals (approval no. SYXK 20170002).

Consent to Participate Not applicable.

Consent for Publication Not applicable.

References

1. Hutson TH, Di Giovanni S (2019) The translational landscape in spinal cord injury: focus on neuroplasticity and regeneration. Nat Rev Neurol 15(12):732–745. https://doi.org/10.1038/s41582-019-0280-3
2. Hu R, Sun H, Zhang Q, Chen J, Wu N, Meng H, Cui G, Hu S, Li F, Lin J, Wan Q, Feng H (2012) G-protein coupled estrogen receptor 1 mediated estrogenic neuroprotection against spinal cord injury. Crit Care Med 40(12):3230–3237. https://doi.org/10.1097/CCM.0b013e3182657560
3. Hu SL, Lu PG, Zhang LJ, Li F, Chen Z, Wu N, Meng H, Lin JK, Feng H (2012) In vivo magnetic resonance imaging tracking of SPIO-labeled human umbilical cord mesenchymal stem cells. J Cell Biochem 113(3):1005–1012. https://doi.org/10.1002/jcb.23432
4. Hu R, Duan B, Wang D, Yu Y, Li W, Luo H, Lu P, Lin J, Zhu G, Wan Q, Feng H (2011) Role of acid-sensing ion channel 1a in the secondary damage of traumatic spinal cord injury. Ann Surg 254(2):353–362. https://doi.org/10.1097/SLA.0b013e31822645b4
5. Chen J, Hu R, Ge H, Duanmu W, Li Y, Xue X, Hu S, Feng H (2015) G-protein-coupled receptor 30-mediated antiapoptotic effect of estrogen on spinal motor neurons following injury and its underlying mechanisms. Mol Med Rep 12(2):1733–1740. https://doi.org/10.3892/mmr.2015.3601
6. Li L, Xiong ZY, Qian ZM, Zhao TZ, Feng H, Hu S, Hu R, Ke Y, Lin J (2014) Complement C5a is detrimental to histological and functional locomotor recovery after spinal cord injury in mice. Neurobiol Dis 66:74–82. https://doi.org/10.1016/j.nbd.2014.02.008
7. Yuan J, Liu W, Zhu H, Chen Y, Zhang X, Li L, Chu W, Wen Z, Feng H, Lin J (2017) Curcumin inhibits glial scar formation by suppressing astrocyte-induced inflammation and fibrosis in vitro and in vivo. Brain Res 1655:90–103. https://doi.org/10.1016/j.brainres.2016.11.002
8. Xia Y, Zhao T, Li J, Li L, Hu R, Hu S, Feng H, Lin J (2008) Antisense vimentin cDNA combined with chondroitinase ABC reduces glial scar and cystic cavity formation following spinal cord injury in rats. Biochem Biophys Res Commun 377(2):562–566. https://doi.org/10.1016/j.bbrc.2008.10.024
9. Xia Y, Yan Y, Xia H, Zhao T, Chu W, Hu S, Feng H, Lin J (2015) Antisense vimentin cDNA combined with chondroitinase ABC promotes axon regeneration and functional recovery following spinal cord injury in rats. Neurosci Lett 590:74–79. https://doi.org/10.1016/j.neulet.2015.01.073
10. Hu SL, Luo HS, Li JT, Xia YZ, Li L, Zhang LJ, Meng H, Cui GY, Chen Z, Wu N, Lin JK, Zhu G, Feng H (2010) Functional recovery in acute traumatic spinal cord injury after transplantation of human umbilical cord mesenchymal stem cells. Crit Care Med 38(11):2181–2189. https://doi.org/10.1097/CCM.0b013e3181f17c0e
11. Chu W, Yuan J, Huang L, Xiang X, Zhu H, Chen F, Chen Y, Lin J, Feng H (2015) Valproic acid arrests proliferation but promotes neuronal differentiation of adult spinal NSPCs from SCI rats. Neurochem Res 40(7):1472–1486. https://doi.org/10.1007/s11064-015-1618-x
12. Chen F, Wang H, Xiang X, Yuan J, Chu W, Xue X, Zhu H, Ge H, Zou M, Feng H, Lin J (2014) Curcumin increased the differentiation rate of neurons in neural stem cells via wnt signaling in vitro study. J Surg Res 192(2):298–304. https://doi.org/10.1016/j.jss.2014.06.026
13. Mekhail M, Almazan G, Tabrizian M (2012) Oligodendrocyte-protection and remyelination post-spinal cord injuries: a review. Prog Neurobiol 96(3):322–339. https://doi.org/10.1016/j.pneurobio.2012.01.008
14. Fehlings MG, Tator CH (1995) The relationships among the severity of spinal cord injury, residual neurological function, axon counts, and counts of retrogradely labeled neurons after experimental spinal cord injury. Exp Neurol 132(2):220–228. https://doi.org/10.1016/0014-4886(95)90027-6
15. Kakulas BA (1999) A review of the neuropathology of human spinal cord injury with emphasis on special features. J Spinal Cord Med 22(2):119–124. https://doi.org/10.1080/10790268.1999.11719557
16. Baumann N, Pham-Dinh D (2001) Biology of oligodendrocyte and myelin in the mammalian central nervous system. Physiol Rev 81(2):871–927. https://doi.org/10.1152/physrev.2001.81.2.871
17. Juurlink BH, Thorburne SK, Hertz L (1998) Peroxide-scavenging deficit underlies oligodendrocyte susceptibility to oxidative stress. Glia 22(4):371–378. https://doi.org/10.1002/(sici)1098-1136(199804)22:4%3c371::aid-glia6%3e3.0.co;2-6
18. Thorburne SK, Juurlink BH (1996) Low glutathione and high iron govern the susceptibility of oligodendroglial precursors to oxidative stress. J Neurochem 67(3):1014–1022. https://doi.org/10.1046/j.1471-4159.1996.67031014.x
19. Fan BY, Pang YL, Li WX, Zhao CX, Zhang Y, Wang X, Ning GZ, Kong XH, Liu C, Yao X, Feng SQ (2021) Liproxstatin-1 is an effective inhibitor of oligodendrocyte ferroptosis induced by inhibition of glutathione peroxidase 4. Neural Regen Res 16(3):561–566. https://doi.org/10.4103/1673-5374.293157
20. Shi J, Tang R, Zhou Y, Xian J, Zuo C, Wang L, Wang J, Feng H, Hu S (2020) Attenuation of white matter damage following deferoxamine treatment in rats after spinal cord injury. World Neurosurg 137:e9–e17. https://doi.org/10.1016/j.wneu.2019.08.246
21. Dixon SJ, Lemberg KM, Lamprecht MR, Skouta R, Zaitsev EM, Gleason CE, Patel DN, Bauer AJ, Cantley AM, Yang WS, Morrison B 3rd, Stockwell BR (2012) Ferroptosis: an iron-dependent form of nonapoptotic cell death. Cell 149(5):1060–1072. https://doi.org/10.1016/j.cell.2012.03.042
22. Feng Z, Min L, Chen H, Deng W, Tan M, Liu H, Hou J (2021) Iron overload in the motor cortex induces neuronal ferroptosis following spinal cord injury. Redox Biol 43:101984. https://doi.org/10.1016/j.redox.2021.101984
23. Chu J, Liu CX, Song R, Li QL (2020) Ferrostatin-1 protects HT-22 cells from oxidative toxicity. Neural Regen Res 15(3):528–536. https://doi.org/10.4103/1673-5374.266060

24. Miotto G, Rossetto M, Di Paolo ML, Orian L, Venerando R, Roveri A, Vučković AM, Bosello Travain V, Zaccarin M, Zennaro L, Maiorino M, Toppo S, Ursini F, Cozza G (2020) Insight into the mechanism of ferroptosis inhibition by ferrostatin-1. Redox Biol 28:101328. https://doi.org/10.1016/j.redox.2019.101328
25. Abdalkader M, Lampinen R, Kanninen KM, Malm TM, Liddell JR (2018) Targeting Nrf2 to suppress ferroptosis and mitochondrial dysfunction in neurodegeneration. Front Neurosci 12:466. https://doi.org/10.3389/fnins.2018.00466
26. Li S, Zhou C, Zhu Y, Chao Z, Sheng Z, Zhang Y, Zhao Y (2020) Ferrostatin-1 alleviates angiotensin II (Ang II)- induced inflammation and ferroptosis in astrocytes. Int Immunopharmacol 90:107179. https://doi.org/10.1016/j.intimp.2020.107179
27. Lu J, Xu F, Lu H (2020) LncRNA PVT1 regulates ferroptosis through miR-214-mediated TFR1 and p53. Life Sci 260:118305. https://doi.org/10.1016/j.lfs.2020.118305
28. Shen L, Lin D, Li X, Wu H, Lenahan C, Pan Y, Xu W, Chen Y, Shao A, Zhang J (2020) Ferroptosis in acute central nervous system injuries: the future direction? Front Cell Dev Biol 8:594. https://doi.org/10.3389/fcell.2020.00594
29. Chen B, Chen Z, Liu M, Gao X, Cheng Y, Wei Y, Wu Z, Cui D, Shang H (2019) Inhibition of neuronal ferroptosis in the acute phase of intracerebral hemorrhage shows long-term cerebroprotective effects. Brain Res Bull 153:122–132. https://doi.org/10.1016/j.brainresbull.2019.08.013
30. Li Y, Liu Y, Wu P, Tian Y, Liu B, Wang J, Bihl J, Shi H (2021) Inhibition of ferroptosis alleviates early brain injury after subarachnoid hemorrhage in vitro and in vivo via reduction of lipid peroxidation. Cell Mol Neurobiol 41(2):263–278. https://doi.org/10.1007/s10571-020-00850-1
31. Xie BS, Wang YQ, Lin Y, Mao Q, Feng JF, Gao GY, Jiang JY (2019) Inhibition of ferroptosis attenuates tissue damage and improves long-term outcomes after traumatic brain injury in mice. CNS Neurosci Ther 25(4):465–475. https://doi.org/10.1111/cns.13069
32. Chen X, Gao C, Yan Y, Cheng Z, Chen G, Rui T, Luo C, Gao Y, Wang T, Chen X, Tao L (2021) Ruxolitinib exerts neuroprotection via repressing ferroptosis in a mouse model of traumatic brain injury. Exp Neurol 342:113762. https://doi.org/10.1016/j.expneurol.2021.113762
33. Qiu Y, Cao Y, Cao W, Jia Y, Lu N (2020) The application of ferroptosis in diseases. Pharmacol Res 159:104919. https://doi.org/10.1016/j.phrs.2020.104919
34. Yumnamcha T, Devi TS, Singh LP (2019) Auranofin mediates mitochondrial dysregulation and inflammatory cell death in human retinal pigment epithelial cells: implications of retinal neurodegenerative diseases. Front Neurosci 13:1065. https://doi.org/10.3389/fnins.2019.01065
35. Basso DM, Beattie MS, Bresnahan JC (1995) A sensitive and reliable locomotor rating scale for open field testing in rats. J Neurotrauma 12(1):1–21. https://doi.org/10.1089/neu.1995.12.1
36. Basso DM, Beattie MS, Bresnahan JC (1996) Graded histological and locomotor outcomes after spinal cord contusion using the NYU weight-drop device versus transection. Exp Neurol 139(2):244–256. https://doi.org/10.1006/exnr.1996.0098
37. Serdar M, Mordelt A, Müser K, Kempe K, Felderhoff-Müser U, Herz J, Bendix I (2019) Detrimental impact of energy drink compounds on developing oligodendrocytes and neurons. Cells. https://doi.org/10.3390/cells8111381
38. Han S, Tang Q, Chen R, Li Y, Shu J, Zhang X (2017) Hepatic iron overload is associated with hepatocyte apoptosis during *Clonorchis sinensis* infection. BMC Infect Dis 17(1):531. https://doi.org/10.1186/s12879-017-2630-3
39. Jiang X, Zhang J, Kou B, Zhang C, Zhong J, Fang X, Huang X, Zhang X, Xie F, Hu Q, Ge H, Yu A (2020) Ambroxol improves neuronal survival and reduces white matter damage through suppressing endoplasmic reticulum stress in microglia after intracerebral hemorrhage. Biomed Res Int 2020:8131286. https://doi.org/10.1155/2020/8131286
40. Muhoberac BB, Vidal R (2019) Iron, ferritin, hereditary ferritinopathy, and neurodegeneration. Front Neurosci 13:1195. https://doi.org/10.3389/fnins.2019.01195
41. Bin JM, Harris SN, Kennedy TE (2016) The oligodendrocyte-specific antibody "CC1" binds quaking 7. J Neurochem 139(2):181–186. https://doi.org/10.1111/jnc.13745
42. Boggs JM (2006) Myelin basic protein: a multifunctional protein. Cell Mol Life Sci 63(17):1945–1961. https://doi.org/10.1007/s00018-006-6094-7
43. Guo Y, Du J, Xiao C, Xiang P, Deng Y, Hei Z, Li X (2021) Inhibition of ferroptosis-like cell death attenuates neuropathic pain reactions induced by peripheral nerve injury in rats. Eur J Pain (London, England) 25(6):1227–1240. https://doi.org/10.1002/ejp.1737
44. Ling X, Liu D (2007) Temporal and spatial profiles of cell loss after spinal cord injury: reduction by a metalloporphyrin. J Neurosci Res 85(10):2175–2185. https://doi.org/10.1002/jnr.21362
45. Ek CJ, Habgood MD, Callaway JK, Dennis R, Dziegielewska KM, Johansson PA, Potter A, Wheaton B, Saunders NR (2010) Spatio-temporal progression of grey and white matter damage following contusion injury in rat spinal cord. PLoS ONE 5(8):e12021. https://doi.org/10.1371/journal.pone.0012021
46. Zhang Y, Fan BY, Pang YL, Shen WY, Wang X, Zhao CX, Li WX, Liu C, Kong XH, Ning GZ, Feng SQ, Yao X (2020) Neuroprotective effect of deferoxamine on erastininduced ferroptosis in primary cortical neurons. Neural Regen Res 15(8):1539–1545. https://doi.org/10.4103/1673-5374.274344
47. Wang J, Chen Y, Chen L, Duan Y, Kuang X, Peng Z, Li C, Li Y, Xiao Y, Jin H, Tan Q, Zhang S, Zhu B, Tang Y (2020) EGCG modulates PKD1 and ferroptosis to promote recovery in ST rats. Transl Neurosci 11(1):173–181. https://doi.org/10.1515/tnsci-2020-0119
48. Ge MH, Tian H, Mao L, Li DY, Lin JQ, Hu HS, Huang SC, Zhang CJ, Mei XF (2021) Zinc attenuates ferroptosis and promotes functional recovery in contusion spinal cord injury by activating Nrf2/GPX4 defense pathway. CNS Neurosci Ther 27(9):1023–1040. https://doi.org/10.1111/cns.13657
49. Guerrero-Hue M, García-Caballero C, Palomino-Antolín A, Rubio-Navarro A, Vázquez-Carballo C, Herencia C, Martín-Sanchez D, Farré-Alins V, Egea J, Cannata P, Praga M, Ortiz A, Egido J, Sanz AB, Moreno JA (2019) Curcumin reduces renal damage associated with rhabdomyolysis by decreasing ferroptosis-mediated cell death. FASEB J 33(8):8961–8975. https://doi.org/10.1096/fj.201900077R